water

MDPI

Article

Realistic Energy, Exergy, and Exergoeconomic (3E) Characterization of a Steam Power Plant: Multi-Criteria Optimization Case Study of Mashhad Tous Power Plant

Mashar Tavana [1], Mahdi Deymi-Dashtebayaz [1,*], Daryoush Dadpour [1] and Behnam Mohseni-Gharyehsafa [2]

[1] Center of Computational Energy, Department of Mechanical Engineering, Hakim Sabzevari University, Sabzevar 9617976487, Iran; mashar3434@gmail.com (M.T.); d.daryoosh2002@gmail.com (D.D.)
[2] Skolkovo Institute of Science and Technology, 3 Nobel Street, Moscow 121205, Russia; mohseni.gharyehsafa.behnam@gmail.com
* Correspondence: m.deimi@hsu.ac.ir or mahdi.deymi@gmail.com

Abstract: This paper presents an in-depth investigation into the performance of Mashhad Tous power plant in Iran, a natural-gas-fueled steam cycle with an output power of 4 × 150 MW. The analyses include energy, exergy, and exergoeconomic. To facilitate the study, a robust code is developed to simulate the thermodynamic topology of the power plant. The fidelity of the simulation is validated using realistic site conditions. The study incorporates three vital decision variables: boiler water mass flow rate, turbine inlet pressure from, and ambient temperature ranging from 90 $kg \cdot s^{-1}$ to 150 $kg \cdot s^{-1}$, 12 MPa to 19 MPa, and 10 °C to 40 °C, respectively. Three different heat loads, including 423 MW, 311 MW, and 214 MW, are used to analyze the performance of the power plant. A Pareto-based multi-criteria optimization intertwined with the technique for order of preference by similarity to the ideal solution (TOPSIS) is used to find the optimum conditions in terms of having the highest work output and exergy efficiency while simultaneously reducing the plant's total cost. The optimization results demonstrate a 4.28% increase in output at full load (423 MW). Additionally, a 1.52% increase is observed at partial load (311 MW), and there is a notable 16% increase in output at low load (214 MW). These improvements also positively impacted energy efficiency. Specifically, there is a 4% improvement at full load, a 0.9% enhancement at partial load, and a remarkable 5.4% increase in energy efficiency at low load. In terms of costs, substantial reductions of 37% at full load, 31% at partial load, and an impressive 72% at low load are evident.

Keywords: steam power plant; exergy; exergoeconomics; heat load; multi-criteria optimization

Citation: Tavana, M.; Deymi-Dashtebayaz, M.; Dadpour, D.; Mohseni-Gharyehsafa, B. Realistic Energy, Exergy, and Exergoeconomic (3E) Characterization of a Steam Power Plant: Multi-Criteria Optimization Case Study of Mashhad Tous Power Plant. *Water* **2023**, *15*, 3039. https://doi.org/10.3390/w15173039

Academic Editor: Gordon Huang

Received: 26 July 2023
Revised: 13 August 2023
Accepted: 15 August 2023
Published: 24 August 2023

1. Introduction

The soaring trend in universal energy consumption, as indicated by the World Energy Council, forecasts a significant surge of over 100% in consumed energy over 40 years [1,2]. Fossil fuels dominate global energy production [3]. Despite improvements in harnessing qualified energies, non-renewable sources will play a pivotal role in meeting humanity's energy needs. Considering the difficulties of the grass-roots design of power plants, including financial restriction, land annihilation, and global warming problems, launching a new power plant may seem a challenging decision. To tackle the issue, retrofitting and finding the optimum site conditions of existing power plants to exploit more energy while simultaneously protecting budgets and the environment has become a topical subject. Thermodynamic analyses are the fundamental aspect of each energy sector. Energy analysis and energy loss are not proper rubrics to justify a system since they do not differentiate between the quality and quantity of energy [4,5]. Exergy is a measure to obtain the maximum amount of producible work of a system. Exergy analysis not only addresses the simple explanation of a system from the energy point of view but further provides additional

notions such as exergoeconomic and exergoenvironmental analyses to characterize an energy sector more deeply [6].

In 2011, Kaushik et al. [7] reviewed in detail energy and exergy analyses in coal- and gas-fired combined power plants. They show that the primary exergy loss occurs in the combustion chamber for gas-fired and the boiler for coal-based power plants. Chen et al. [8] investigated the thermodynamic performance of a hybrid system consisting of a gas turbine, a tubular solid oxide fuel cell, and hydrogen fuel. Their obtained results indicated that an increase in the turbine's inlet temperature leads to a decrease in the system efficiency, yet the power generation of the system increases. Furthermore, raising the turbine's inlet temperature and increasing the pressure ratio result in higher entropy and system instability. At the design point, the efficiency of the hybrid system was 9.81%, whereas the efficiency of the system without a fuel cell was 33.4%. Amiralipour and Kouhikamali [9] simulated the retrofitting procedure of a combined steam power plant in Guilan by integrating a cooling water pump (CWP) accompanied with membrane and thermal distillation units. The power plant has a nominal electricity output of 450 MW. They presented two distinct scenarios, including the high-pressure line (HP) and low-pressure line (LP) of the heat recovery steam generator (HRSG) for water production, where the former produces about 25,000 m^3, while the latter leads to 7000 m^3. Considering their economic analysis, the price of the produced fresh water is from 2.5 USD/m^3 to 3 USD/m^3. Lin et al. [10] analyzed the utilization of a steam air heater (SAH) to exploit the waste heat of a 1000 MW single-reheat supercritical coal-fired power plant. They investigated the performance of the power plant using thermoeconomic analysis. The results imply that the payback periods for the three different case studies, including bypass flue (BPF), BPF-SAH, and BPF-SAHs, are 2.75 years, 3.42 years, and 2.36 years. In another study, Owebor et al. [11] investigated a fully integrated combined cooling heat and power system comprising a gas turbine, solid oxide fossil fuel, a steam turbine, an organic Rankine cycle, and absorption refrigeration followed by cryogenic carbon capture and storage with a thermoeconomic and environmental approach. The net power of the complex is 147.2 MW and the exergy efficiency of their system is 39.9%. The results show a levelized energy cost and investment payback period of 0.123 USD/kWh and 5.2 years, respectively. Zahedi et al. [12] assessed a quaternary combined power plant comprising a solar-integrated Brayton cycle, biogas Brayton cycle, organic Rankine cycle, and steam gas cycle. The genetic optimization algorithm was used to find the optimum site condition of the combined power plants: the exergy efficiency of the optimum condition is 61.6%, and the electricity generation cost is 0.0636 USD per kilowatt-hour. A carbon capture section, carbon amine adsorption type, was also added to the system, which decreased the system's exergy to 50.5%. Abbaspour et al. [13] explored the thermodynamic efficiencies of a multi-generation energy system, including a gas cycle, steam cycle, cryogenic air separation, proton exchange membrane, electrolyzer, and ammonia–urea reactor. The simulations imply 689 GWh and 1.323 million tons of urea production yearly with a net present value of USD 7.29 billion.

Topal et al. [14] conducted an energy and exergy analysis of a biomass co-firing power plant using olive pits in a can circulating fluidized bed power plant in Turkey. The exergy efficiency of this 157 MW electricity output plant is about 31.26%. Moreover, they concluded that increasing the turbine inlet temperature and pressure and the temperature of the compressed air and feed water leads to lower CO_2 emissions. Mohammadpour et al. [15] performed an energy and exergy (2E) analysis for an oxy-fuel regenerative gas turbine. They considered two distinct streams for CO_2, including primary and dilution. The highest exergy destruction in the system happens in the combustion chamber. In another investigation, Abuelnuor et al. [16] applied fundamental 2E thermodynamic analysis in a 180 MW combined power plant in Khartoum. The energy and exergy efficiency of the power plant were 38% and 49%. Bai et al. and Yan et al. [17,18] tried to investigate the performance of coal-fired power plants based on 2E thermodynamic analyses. The former study reported 1.046% exergy efficiency increase after enhancing the recompression supercritical CO_2 cycle; the total exergy, energy, and power efficiency were 53.41%, 94.68%, and 48.06%. The latter

work simulated the integration of a trough collector system in a coal-fired power plant with a nominal electricity output of 660 MW. The exergy efficiency of the combined system highly depends on daily solar irradiance. With 300 $W \cdot m^{-2}$ variations in the solar intensity, the exergy efficiency fluctuates from about 33% to 57%. In [19], a geothermal power plant accompanied by non-condensable gases in two distinct site conditions, including subcritical and supercritical, was analytically investigated. The exergy efficiencies of the subcritical and supercritical modes were 50.5% and 52%, respectively. They concluded that turbine inlet pressure has an indirect relation with the exergy performance of the supercritical cycle, while the subcritical cycle's performance first increases and then reduces. The analysis reveals the levelized cost of energy for the subcritical and supercritical systems by 5.52 $EUR \cdot KWh^{-1}$ and 6.96 $EUR \cdot KWh^{-1}$, respectively. Elhelw and Al Dahma [20] studied the exergetic performance of the new Abu Qir thermal steam power plant in Alexandria with 650 MW nominal output power. The investigation was divided into full and half loads. The exergy destruction share of the boiler, turbine, and condenser is 75%, 15%, and 6%, respectively. The half load's exergy destruction for the same devices in order is 78%, 14%, and 5%. Khaleel et al. [21] studied the energy and exergy performance of a steam coal-fired power plant. The sensitivity analysis of the superheater pressure and temperature was investigated. Doubling the superheater pressure leads to enhanced net power output by about 8%. The superheater temperature had the same trend. Increasing the steam temperature from 539.8 to 580 °C, the net power increases by 6%. The overall energy and exergy efficiencies of this 589.47 MW power plant are 30.41% and 62.20%, respectively. Ahmadi et al. [22] used energy, exergy, and exergoenvironmental analyses to evaluate the performance of a CHP power plant in Isfahan Petrochemical Complex, Iran. The complex aims to generate Benzene, Orthoxylene, Toluene, and Xylene. The CHP's net power is about 18 MW. The energy and exergy efficiency of the plant are 8.22% and 7.87%. The boiler possesses the highest exergy destruction rate at 65,571 kW. Adnan et al. [23] delved into two waste fuel power plants in two cities in Bangladesh. Taking 3 million metric tons (MMT) of municipal solid waste, Dhaka's power plant's net power is 169 MW, and Chattogram's output is 83 MW. The environmental analysis shows that burning solid waste curbed carbon emissions by about 1 MMT for Dhaka and 0.5 MMT for Chattogram. Hao et al. [24] conducted an energy and exergy analysis, along with an economic exergy analysis, of Huadian Kemen Power Plant based on its operational efficiency and its impact on the discharged heat to the surrounding environment. Their findings indicated that the construction of heat-retaining and -diversion facilities within the power plant reduced the intake water temperature and improved heat distribution, although regions with higher temperatures also experienced an increase.

Given the paramount importance of exergy analysis evident in the reviewed literature above, this investigation evaluates the thermodynamic performance of a potential and strategic power plant in Iran: Mashhad Tous power plant. The thermodynamic analyses consist of energy, exergy, and exergoeconomic, which is the translation of exergy into economic notions. Regardless of most of the literature mimicking power plant systems through simulation, this work peruses the thermodynamic efficiencies completely using the experimental data log from the site. Three pivotal parameters, mass flow rate of the water inlet to the boiler, turbine steam inlet pressure, and ambient temperature, are considered the power plant's input variables. The optimum working condition to maximize the network output and exergetic performance while simultaneously curbing the system's cost is applied using Pareto-based multi-criteria. Some notable novelties of the present study are as follows:

- Utilizing energy, exergy, and ecoexergy equations for the Tous power plant;
- Optimizing effective parameters through a multi-objective optimization method;
- The best ambient temperature has been selected based on exergy efficiency, work, and capital cost under various loads;
- Employing experimental results for the validation and modeling of a power plant.

2. Materials and Methods

2.1. Mashhad Tous Power Plant Topology

The Mashhad Tous power plant is in Mashhad, the center of Khorasan Razavi province in Iran. The plant consists of four identical sections, each of which with 150 MW power output. The plant's operation conditions are comprehensively tabulated in Table 1.

Table 1. Power plant's operating conditions.

Operating Conditions	Value
Power produced	150 (MW)
Mass flow rate of fuel	39.8 ($N{\cdot}m^3{\cdot}h^{-1}$)
Stack flue gas temperature	110 (°C)
Steam temperature, main line	540 (°C)
Steam flow rate, main line	520 ($Ton \cdot h^{-1}$)
Number of induced and draft fans	2
Number of burners	9
Pump/motor efficiency	95%

The steam Rankine cycle is employed for the Tous power plant, fueled by natural gas. Figure 1 shows the thermodynamic cycle of the power plant. Point 1 is the place where water enters the boiler with a temperature of 243 °C and a pressure of 13.684 MPa. Superheated steam leaves the boiler at point 2 with a temperature of 538 °C and pressure of 12.919 MPa. After shaft power generation in the high-pressure turbine, the steam's temperature and pressure are reduced to 355 °C and 3.633 MPa. Prior to entering the intermediate pressure turbine, the steam is reheated via exploiting the boiler's heat shown at point 5. The reheated steam leaves the boiler at 538 °C and 3.239 MPa. The steam enters the intermediate pressure turbine at point 6, and before entering the condenser, the steam releases its enthalpy via expansion in a low-pressure turbine.

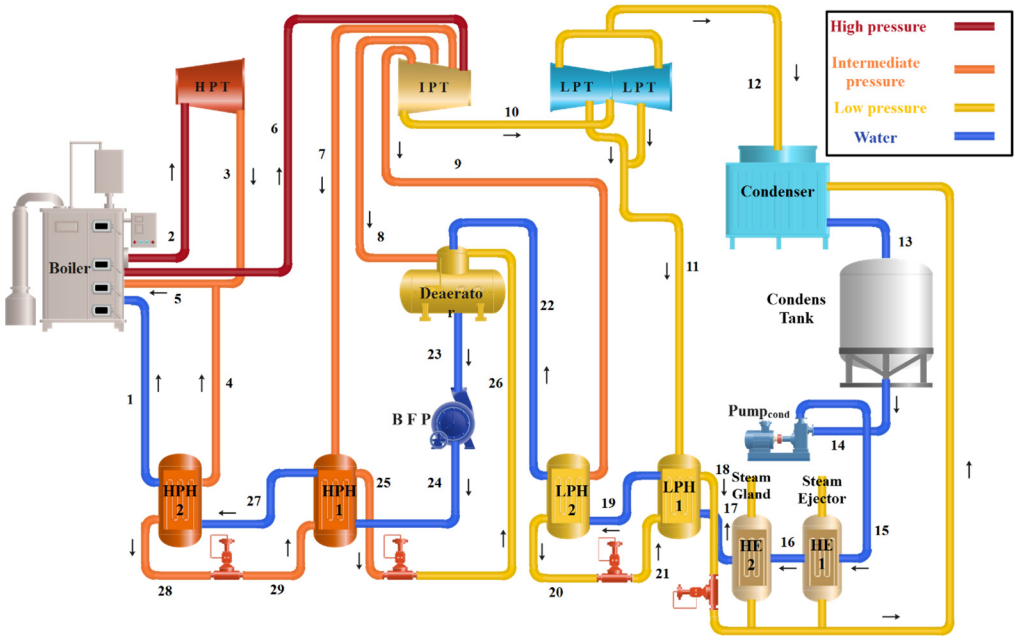

Figure 1. Topology of the power plant.

The condensation process in the Tous power plant is the air-cooled type. The low-pressure steam enters the condenser at point 12, and the resultant condensate goes to the tank at point 13. The leaving water from the condensate tank has a temperature of about 45 °C. The condensate pump increases the water pressure up to 1.358 MPa. The pressurized water passes through low-pressure heaters, leading to a temperature of 132 °C at point

22. Then, through receiving heat energy in the deaerator, the temperature meets 170 °C. The boiler feed pump at point 24 soars the pressure up to 17.732 MPa. Two high-pressure heaters are aimed to intensify the temperature of the steam, where it reaches 243 °C at point 1. The energy required to increase the temperature of water in the two phases, water and steam, is obtained through steam removal from the turbines at different points, including 3, 4, 5, 6, 7, 8, and 9. Table 2 provides the thermodynamic details of the cycle: temperature, pressure, mass flow rate, enthalpy, entropy, and specific exergy from the site measurements. The fundamental thermodynamic analyses, including energy and exergy, are explained in the following section.

Table 2. Thermodynamic properties of the Tous power plant, site conditions measurements.

Points	T (°C)	P (MPa)	$\dot{m}$ (kg·s^{-1})	h (kJ·kg^{-1})	s (kJ·kg^{-1}·K^{-1})	ex (kJ·kg^{-1})
1	243	13.684	145	1053	2.707	889.3
2	538	12.919	145.1	3439	6.571	3179
3	355	3.633	145.1	3113	6.656	2851
4	353	3.627	10.1	3108	6.649	2846
5	353	3.544	132.1	3110	6.662	2848
6	538	3.239	135	3540	7.304	3261
7	452	1.804	7.6	3365	7.341	3085
8	356	0.837	7.44	3173	7.407	2892
9	244	0.3201	8.01	2954	7.461	2672
10	226	0.2686	110	2920	7.473	2637
11	128	0.09225	4.7	2733	7.545	2449
12	65	0.02482	99	2618	7.833	2326
13	63	0.05572	112.5	263.7	0.8687	146.3
14	65	0.056	113.3	272.1	0.8935	154.1
15	66	1.358	113.3	277.4	0.9051	159.1
16	67.5	1.317	113.3	283.6	0.9236	164.8
17	69.7	1.2	113.3	292.7	0.9506	173.3
18	95	0.08825	12.8	398	1.25	271.1
19	92.5	1.114	113.3	388.3	1.221	262.1
20	134	0.3157	8.01	563.5	1.677	425.9
21	134	0.08825	7.7	2745	7.596	2460
22	132	1.280	113.3	555.6	1.655	418.6
23	170	0.8374	133	719.3	2.042	572.6
24	173.5	17.732	133	743.9	2.055	596.8
25	178.5	1.753	17.1	757	2.124	608.3
26	178	1.540	17.09	754.7	2.119	606.1
27	207	15.401	133.7	889.3	2.375	734.3
28	212	3.527	10.3	907.3	2.441	750.6
29	207	1.752	10.13	2799	6.395	2544

2.2. Thermodynamic Modeling

2.2.1. Energy and Exergy Analysis

To analyze a system from the thermodynamic point of view, the control volume hypothesis is applied through the system. The general form of the mass and energy balance over a control volume is encapsulated by the following overarching principles [25]:

$$\sum \dot{m}_{in} - \sum \dot{m}_{out} = 0 \quad (1)$$

$$\dot{Q} - \dot{W} + \sum \dot{m}_{in} h_{in} - \sum \dot{m}_{out} h_{out} = 0 \quad (2)$$

where $\dot{m}$, $\dot{Q}$, $\dot{W}$, and h are the mass flow rate, heating power, mechanical power output, and enthalpy. The subscripts i and o elegantly mark the inlet and outlet of a given control volume.

The foundational first law of thermodynamics asserts that energy will not be lost; this law does not explain energy conversion inside a control volume. In contrast, exergy analysis derived from the second law of thermodynamics perfectly addresses the energy disappearance and maximum obtainable work of an energy flow. The general form of the exergy balance is concisely expressed through the following relationship [26].

$$\sum \dot{m}_{in} ex_{in} - \sum \dot{m}_{out} ex_{out} + \dot{E}x_Q - \dot{E}x_W - \dot{E}x_D = 0 \quad (3)$$

where ex is the specific exergy, $\dot{E}x_Q$ denotes the exergy rate of the heat transfer, $\dot{E}x_W$ is the exergy due to work, and $\dot{E}x_D$ is the rate of exergy destruction. The following formula characterizes the abovementioned terms. The subscript 0 signifies the reference condition [27].

$$ex = (h - h_0) - T_0(s - s_0) \quad (4)$$

$$\dot{E}x_Q = Q\left(1 - \frac{T_0}{T}\right) \quad (5)$$

$$\dot{E}x_W = \dot{W} \quad (6)$$

The total amount of the exergy of a flow reads

$$\dot{E}x_{total} = \dot{m}((h - h_0) - T_0(s - s_0)) \quad (7)$$

The energy and exergy balance for each piece of equipment in the cycle is tabulated in Table 3. Notably, the terms η_{en} and η_{ex} indicate the corresponding energy and exergy efficiencies.

2.2.2. Exergoeconomic Analysis

Changes in an energy system need a careful cost analysis for each ingredient inside the system. Exergy analysis lays the foundation for a precise economic investigation, called exergoeconomic analysis. Exergoeconomics provides economic value to a specific exergy flow. Exergoeconomic analysis identifies the final cost of each product separately, ranging from the actual cost of the product or service, the investment cost of the system, assembly cost, fuel cost, and labor remuneration, to the operating and maintenance (O&M) cost for a multi-output multi-input energy system. Moreover, provides a reliable basis to find the place, reason, and value of losses, leading to comprehensive cost optimization [29].

Table 3. Equipment energy and exergy equations [28].

Equipment	Energy and Exergy Formula
Boiler	$\dot{Q}_{Boiler} = \dot{m}_1(h_2 - h_1) + \dot{m}_5(h_6 - h_5)$ $\dot{Q}_{fuel} = \dot{m}_{fuel} \cdot \psi_{fuel}$ $\eta_{en,\ Boiler} = \frac{\dot{m}_1(h_2 - h_1) + \dot{m}_5(h_6 - h_5)}{\dot{Q}_{fuel}}$ $\eta_{ex,\ Boiler} = \frac{\dot{m}_1(ex_2 - ex_1) + \dot{m}_5(ex_6 - ex_5)}{\dot{Q}_{fuel}\left(1 - \frac{T_0}{T_b}\right)}$
Turbine	$\dot{W}_{Turbine,\ hp} = \dot{m}_2(h_2 - h_3)$ $\eta_{en,\ Turbine,\ hp} = \frac{\dot{W}_{turbine,\ hp}}{\dot{m}_2(h_2 - h_3)}$ $\eta_{ex,\ Turbine,\ hp} = \frac{\dot{W}_{turbine,\ hp}}{\dot{m}_2(ex_2 - ex_3)}$ $Ex_{D,\ Turbine,\ hp} = \dot{m}_2(ex_2 - ex_3) - \dot{W}_{Turbine,\ hp}$
Condenser	$\dot{Q}_{Condenser} = \dot{m}_{12}(h_{12} - h_{13})$ $Ex_{D,\ Condenser} = \dot{m}_{12}(ex_{12} - ex_{13}) - \dot{Q}_{Condenser}\left(1 - \frac{T_0}{T_c}\right)$

Table 3. *Cont.*

Equipment	Energy and Exergy Formula
BFP	$\dot{W}_{BFP} = \dot{m}_{23}(h_{24} - h_{23})$ $\eta_{en,\ BFP} = \frac{\dot{m}_{23}(h_{24}-h_{23})}{\dot{W}_{BFP}}$ $\eta_{ex,\ BFP} = \frac{\dot{m}_{23}(ex_{23}-ex_{24})}{\dot{W}_{BFP}}$
$Pump_{cond}$	$\dot{W}_{Pump_{cond}} = \dot{m}_{14}(h_{15} - h_{14})$ $\eta_{en,\ Pump_{cond}} = \frac{\dot{m}_{14}(h_{15}-h_{14})}{\dot{W}_{Pump_{cond}}}$ $\eta_{ex,\ Pump_{cond}} = \frac{\dot{m}_{14}(ex_{15}-ex_{14})}{\dot{W}_{Pump_{cond}}}$
Deaerator	$\eta_{en,\ Deaerator} = \frac{\dot{m}_{23}h_{23}}{\dot{m}_8h_8+\dot{m}_{22}h_{22}+\dot{m}_{26}h_{26}}$ $\eta_{ex,\ Deaerator} = \frac{\dot{m}_{23}ex_{23}}{\dot{m}_8ex_8+\dot{m}_{22}ex_{22}+\dot{m}_{26}ex_{26}}$ $Ex_{D,\ Deaerator} = \dot{m}_8ex_8 + \dot{m}_{22}ex_{22} + \dot{m}_{26}ex_{26} - \dot{m}_{23}ex_{23}$

According to the Specific Exergy Costing approach (SPECO) [30], exergoeconomic analysis includes three steps: 1/finding the exergy flows, 2/characterizing the input and output of each piece of equipment, and 3/developing a cost balance. The exergoeconomic balance of a component is described as follows [31]:

$$\sum \dot{C}_{in,k} - \sum \dot{C}_{out,k} + \sum \dot{C}_{Q,k} - \sum \dot{C}_{W,k} + \sum \dot{Z}_{Total,k} = 0 \quad (8)$$

where $\dot{C}_{in,k}$, $\dot{C}_{out,k}$, $\dot{C}_{Q,k}$, $\dot{C}_{Q,k}$, $\dot{C}_{W,k}$, and $\dot{Z}_{Total,k}$ for component k indicate the exergy cost rate of an inlet exergy stream, the exergy cost rate of an outlet exergy stream, the cost rate of the exergy associated with heat transfer, the cost rate of the exergy associated with work, and the total cost rate consisting of the capital investment and the operating and maintenance cost, respectively. These cardinal parameters are articulated through Equations (9) to (12) [32].

$$\dot{C}_{in} = c_{in}\dot{E}x_{in} \quad (9)$$

$$\dot{C}_{out} = c_{out}\dot{E}x_{out} \quad (10)$$

$$\dot{C}_{Q} = c_{Q}\dot{E}x_{Q} \quad (11)$$

$$\dot{C}_{W} = c_{W}\dot{E}x_{W} \quad (12)$$

The capital investment of each component is calculated with the capital function provided in the literature and a parameter called capital recovery factor (CRF) [33]. The capital recovery factor can be obtained using the values of interest rate (i) and component operating years (n). In the current investigation, the interest rate is taken as 0.1 for 20 years of operation. The operating and maintenance cost is calculated as a percentage of the cost of each component based on the parameter γ_k; in this investigation, γ_k is considered as 1.06. Equations (13)–(16) indicate the details of obtaining the total cost rate for component k [32].

$$\dot{Z}_{Total} = \dot{Z}_k^{CI} + \dot{Z}_k^{OM} \quad (13)$$

$$\dot{Z}_k^{CI} = \left(\frac{CRF}{\tau}\right) Z_k \quad (14)$$

$$CRF = \frac{i(1+i)^n}{(1+i)^n - 1} \quad (15)$$

$$\dot{Z}_k^{OM} = \gamma_k Z_k \quad (16)$$

The capital functions for each component, Z_k, are tabulated in Table 4 [29,34]. The components include a boiler, turbine, condenser, pump, deaerator, and heater. The cost balance provided by the auxiliary equations is tabulated in Table 5.

Table 4. Capital function for components.

Component	Cost Function
Boiler	$Z_{Boiler} = a_1 (\dot{m}_1)^{a_2} \beta_p \beta_T \beta_\eta \beta_{SH/RSH}$ $\beta_p = \exp\left(\frac{P_2 - \bar{P}_e}{a_3}\right)$, $\beta_T = 1 + a_5 \exp\left(\frac{T_2 - \bar{T}_e}{a_6}\right)$, $\beta_{eta} = 1 + \left(\frac{1-\bar{\eta}_1}{1-\eta_1}\right)^{a_4}$ $\beta_{SH/RSH} = 1 + \frac{T_2 - T_1}{T_2} + \frac{\dot{m}_6}{\dot{m}_1}\frac{T_6 - T_5}{T_6}$ $\bar{T}_e = 593\ (^\circ C)$, $\bar{P}_e = 28\ (bar)$, $\bar{\eta}_1 = 0.9$, $a_1 = 208,582\ (\$ \cdot kg^{-1} \cdot s^{-1})$ $a_2 = 0.8$, $a_3 = 150\ (bar)$, $a_4 = 7$, $a_5 = 5$, $a_6 = 10.42\ (^\circ C)$
Turbine	$Z_{Turbine} = a_7 \dot{W}_{Turbine}^{0.7} \left(1 + \left(\frac{0.05}{1-\eta_{Turbine}}\right)^3\right)\left(1 + 5\exp\left(\frac{T_{in} - 866\ K^{-1}}{10.42\ K^{-1}}\right)\right)$ $a_7 = 3880.5\ (\$ \cdot kW^{-0.7})$
Condenser	$Z_{Condenser} = 1773 \dot{m}_{12}$
BFP/$Pump_{cond}$	$Z_{Pump} = 705.48 \dot{W}_{Pump}^{0.71} \left(1 + \left(\frac{0.2}{1-\eta_{Pump}}\right)\right)$
Deaerator	$Z_{Deaerator} = a_8 \dot{m}_{22}^{a_9}$ $a_8 = 143,315\ (\$ \cdot kW^{-0.7})$, $a_9 = 0.7$
Heaters (LPH1, LPH2, HPH1, HPH2, HE1, and HE2)	$Z_{Heater} = 2020 \times 3.3Q\left(\frac{1}{T_D}\right)^{0.1} (10\Delta P_t)^{-0.08} (10\Delta P_s)^{-0.04}$

Note(s): Q is the rate of heat transfer in the feed water heater (kW); T_D is the difference between the saturated temperature of the steam extracted from the turbine and the temperature of the outlet feed water in the feed water heater (°C); $\triangle P_t$ and $\triangle P_s$ are the pressure drop in the feed water heater and the extraction steam of the feed water heater, respectively (MPa).

Table 5. Cost balance and auxiliary equations [35].

Component	Equation
Boiler	$c_{fuel}\dot{E}x_{fuel} + Z_{Boiler} = c_2\dot{E}x_2 - c_1\dot{E}x_1 + c_6\dot{E}x_6 - c_5\dot{E}x_5$ $c_6 = c_2$
Turbine	$c_2\dot{E}x_2 - c_4\dot{E}x_4 - c_5\dot{E}x_5 + \dot{Z}_{Turbine} = c_{Work}\dot{E}x_{Work,\ Turbine}$ $c_4 = c_2$, $c_5 = c_2$
Condenser	$c_{12}\dot{E}x_{12} + \dot{Z}_{condenser} = c_{13}\dot{E}x_{13}$ $c_{13} = c_{14}$
BFP	$c_{23}\dot{E}x_{23} + \dot{Z}_{BFP} + c_{work}\dot{E}x_{Work,\ BFP} = c_{24}\dot{E}x_{24}$
$Pump_{cond}$	$c_{14}\dot{E}x_{14} + \dot{Z}_{Pump_{cond}} + c_{work}\dot{E}x_{Work,\ pump_{cond}} = c_{15}\dot{E}x_{15}$
Deaerator	$c_8\dot{E}x_8 + c_{26}\dot{E}x_{26} - c_{23}\dot{E}x_{23} + \dot{Z}_{Deaerator} = c_{23}\dot{E}x_{23} - c_{22}\dot{E}x\_22$ $c_{23} = c_{22}$
Heater	$c_9\dot{E}x_9 + \dot{Z}_{Heater} - c_{20}\dot{E}x_{20} = c_{22}\dot{E}x_{22} - c_{19}\dot{E}x_{19}$ $c_{20} = c_{19}$

Table 6 displays the exergoeconomic parameters such as relative cost, fuel cost, and product cost, and, using these relationships, their values can be calculated.

Table 6. Exergoeconomic parameters [36].

Parameter	Equation
Average cost per unit exergy of fuel	$c_{F_k} = \frac{\dot{C}_{F_k}}{\dot{E}_{F_k}}$
Average cost per unit exergy of product	$c_{P_k} = \frac{\dot{C}_{P_k}}{\dot{E}_{P_k}}$
Cost rate of exergy destruction	$\dot{C}_{D_k} = c_{F_k}\dot{E}_{D_k}$
Exergoeconomic factor	$f_k = \frac{\dot{Z}_k}{\dot{Z}_k+\dot{C}_{D_k}}$
Relative cost difference (%)	$r_k = \frac{c_{P_k}-c_{F_k}}{c_{F_k}} * 100$

2.3. Multi-Criteria Optimization

Any attempts at optimization in the energy industry call for a careful decision in terms of achieving maximum efficiency, such as output power, while reducing cost simultaneously. In the current investigation, the goal is to find the maximum exergy efficiency and net power output with the lowest total cost. Multi-criteria optimization methods may provide a suitable answer for these kinds of problems. In the Pareto-based multi-criteria approach, the goal is to find a series vector consisting of design variables (X) satisfying m inequality constraints and n equality constraints. The formulae are described in Equations (17) and (18), respectively [37].

$$g_i(X) \leq 0,\ i = 1,\ 2,\ \cdots,\ m \tag{17}$$

$$f_i(X) = 0,\ i = 1,\ 2,\ \cdots,\ n \tag{18}$$

In multi-criteria optimization problems, usually, outputs' trends are against each other. Put succinctly, in a specific set of decision variables, one output is the maximum, while the others show the minimum amount. Therefore, there should be a set of solutions that satisfies the needed optimum criteria. This set of solutions is called the Pareto front. The optimum solutions inside the Pareto front dominate all other possible solutions.

In the current study, the thermodynamic cycle of the Mashhad Tous power plant is simulated and validated with the experimental data log obtained from the site. Robust exergy and exergoeconomic codes are developed to analyze the performance of the power plant. Three distinct input parameters are chosen, including the ambient temperature, mass flow rate to the boiler, and HP turbine inlet pressure, as a case study. The results are explained in detail, and the technique for order of preference by similarity to the ideal solution (TOPSIS) method [38] is employed to reveal the most optimum conditions for each investigated case study to achieve the highest exergy efficiency and work output at the lowest total cost. The flowchart of the current study is shown in Figure 2.

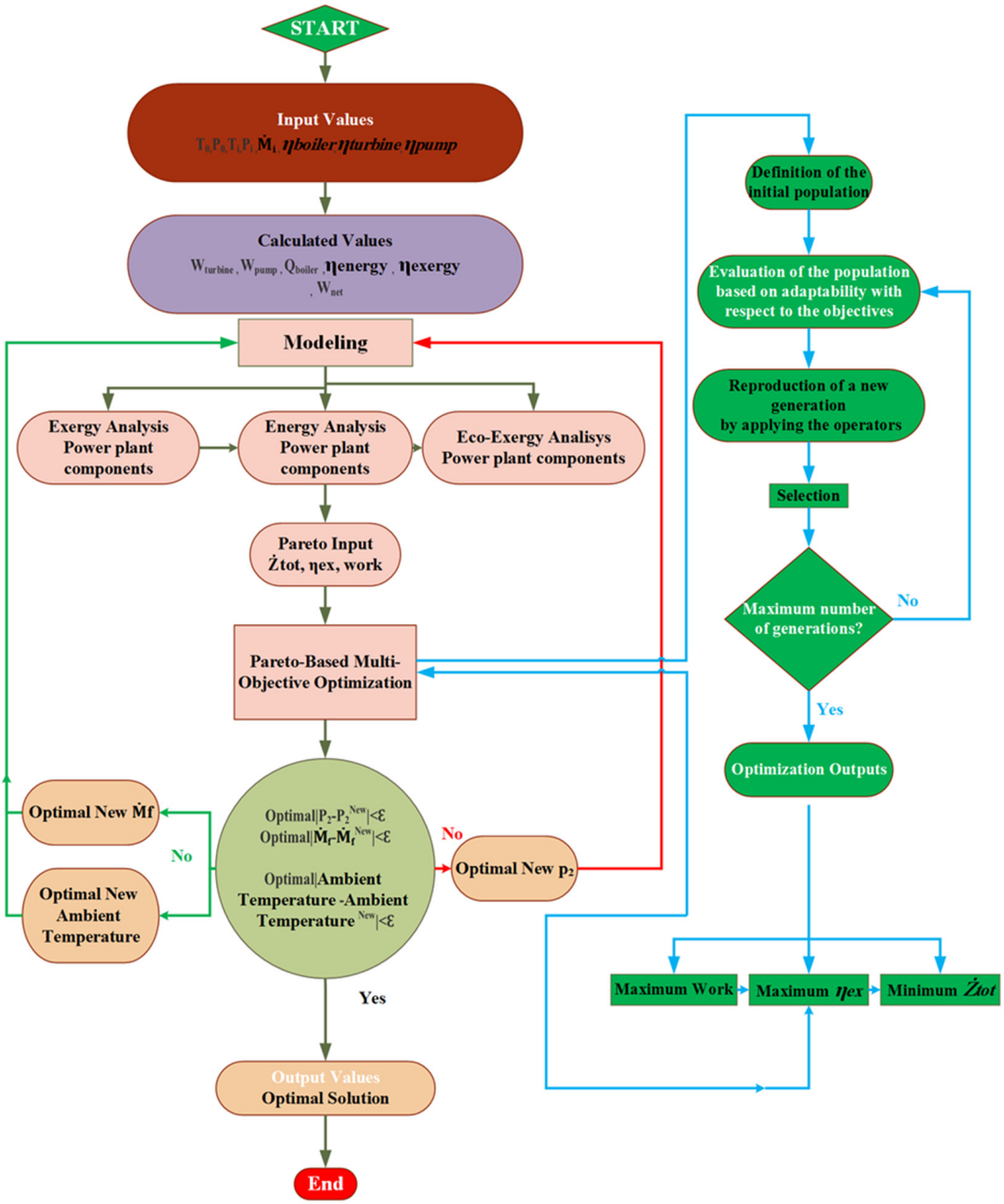

Figure 2. Flowchart for finding the optimum conditions for Mashhad Tous power plant.

3. Results

The result of this study is compartmentalized into four distinct sections: 1/validation, 2/energy and exergy analysis, 3/exergoeconomic results, and 4/optimization.

3.1. Validation

The simulation of the power plant cycle is validated using actual work, as shown in Table 7. The power plant's output power was extracted from its data sheets, and these values were compared with the calculated power. Table 7 depicts the actual work versus the calculated power output for different heat loads: $\dot{Q}_H$ = 214 MW, $\dot{Q}_H$ = 311 MW, and $\dot{Q}_H$ = 423 MW at 28 °C and 12.76 MPa.

Table 7. Validation of Mashhad Tous power plant simulation.

Heat Load (MW)	Site Actual Work (MW)	Calculated Work (MW)
214	75	76.259
311	112.5	123.053
423	150	154.377

3.2. Energy and Exergy Results

Figure 3 illustrates the variation in energy efficiency (η_{en}) and work output ($\dot{W}_{net}$) against the inlet pressure of the high-pressure turbine (P_2). Increasing the pressure for each three heat load categories leads to lower work output and energy efficiency. As an example, by increasing the pressure by about 7 MPa from the point P_2 = 12 MPa at the heat load of $\dot{Q}_H$= 214 MW, the energy efficiency dropped by 3.74%. At constant pressure, providing more heat to the boiler results in gaining more work output. At P_2 = 19 MPa, if the heat load increases from 214 MW to 423 MW, the work output soars twofold and reveals 150.6 MW. The energy efficiency trend, assuming that the boiler heat load is at constant pressure, first increases then reduces; increasing the heat load from 214 MW to 311 MW at P_2 = 15 MPa, the energy efficiency sharply advances relatively by about 12.9%, while further increasing the heat load to the third step shrinks the efficiency by about 7.58%. Maximum work output occurs at the pressure of 12 MPa and heat load of 423 MW. The highest energy efficiency is at 12 MPa and a heat load of 311 MW.

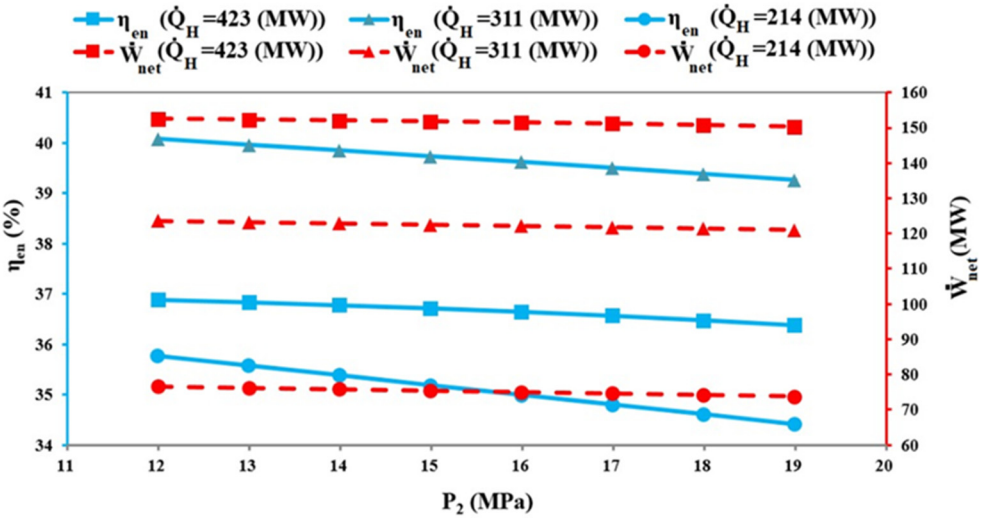

Figure 3. Variation in energy efficiency and work output with HP turbine inlet pressure.

Figure 4 delves into the sensitivity of the energy efficiency and work output to the boiler water flow rate. Increasing the water discharge in each heat load is accompanied by more net power output and more energy efficiency. When the mass flow rate of the feed water increases from 90 $kg \cdot s^{-1}$ to 150 in the heat load of 311 MW, the work output extends to 44.43 MW. Here, the energy efficiency is 20.84% at the same heating load condition. At a constant mass flow rate, the work output of the medium heating load, 311 MW, possesses the lowest figure compared to the other loads. The highest heating load of 423 MW for the mass flow rate between 90 $kg \cdot s^{-1}$ and 130 $kg \cdot s^{-1}$ dominates the intermediate load in terms of work output, while this trend is reversed when the mass flow increases up to 150 $kg \cdot s^{-1}$ under the same condition. The intermediate heating load has the highest energy efficiency at each mass flow rate. The maximum energy efficiency and work output take place at $\dot{m}_f$ = 150 $kg \cdot s^{-1}$ for $\dot{Q}_H$ = 311 MW and $\dot{Q}_H$ = 214 MW, respectively.

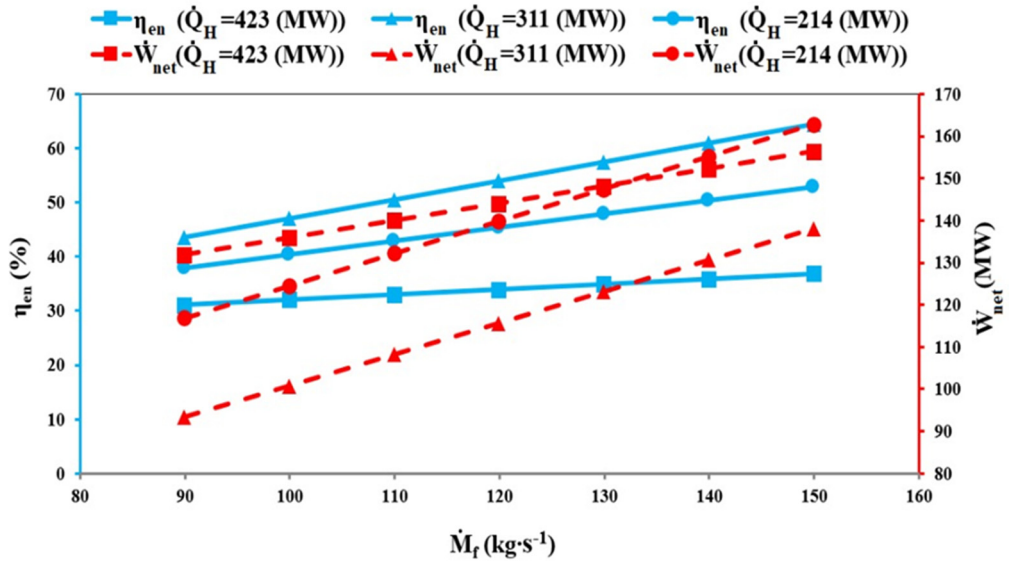

Figure 4. Variation in energy efficiency and work output with boiler water flow rate.

The influence of ambient temperature on energy efficiency and work output is illustrated in Figure 5. The energy efficiency of the power plant is inversely related to the ambient temperature for each heat load. Doubling the ambient temperature at the intermediate heat load linearly decreases the energy efficiency by 2.13%. The sensitivity of energy efficiency to the ambient temperature for the heat loads of 214 MW and 423 MW is lower than that for the intermediate load. Increasing the temperature for the heat loads of 311 MW and 423 MW leads to lower work output; however, for the heating load of 214 MW, the power plant produces slightly more work output. For instance, if the ambient temperature quadruples from the initial value of 10 °C, the cycle provides 0.3 MW more work output.

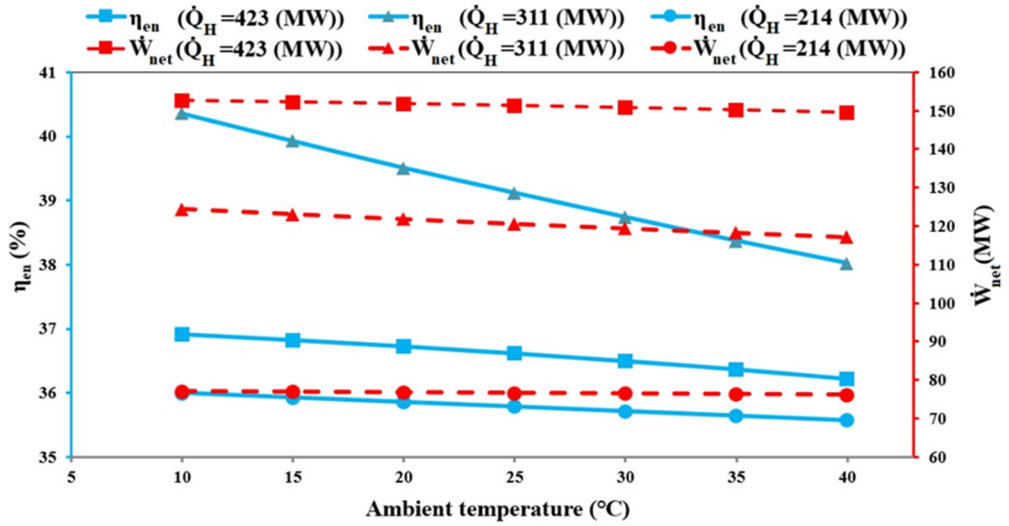

Figure 5. Variation in energy efficiency and work output with ambient temperature.

Applying the exergy balance to the three distinct heat sources and initial conditions, the rate of total exergy destruction can be obtained. Figure 6A,B show the exergy destruction rate for different heat loads against the inlet pressure of the HP turbine and the ambient temperature, respectively. According to the figures, the more heat loads provided, the more exergy is destructed. Increasing the inlet pressure results in higher exergy destruction. For the heat load of 423 MW, if the pressure increases from 12 MPa to 19 MPa, about 11.5 MW more exergy will be destructed. The exergy destruction profile is less sensitive to ambient temperature compared with turbine pressure. As an example, a fourfold increase

in ambient temperature from the initial point at 10 °C leads to 6.6 MW more destructive exergy at the same heat load.

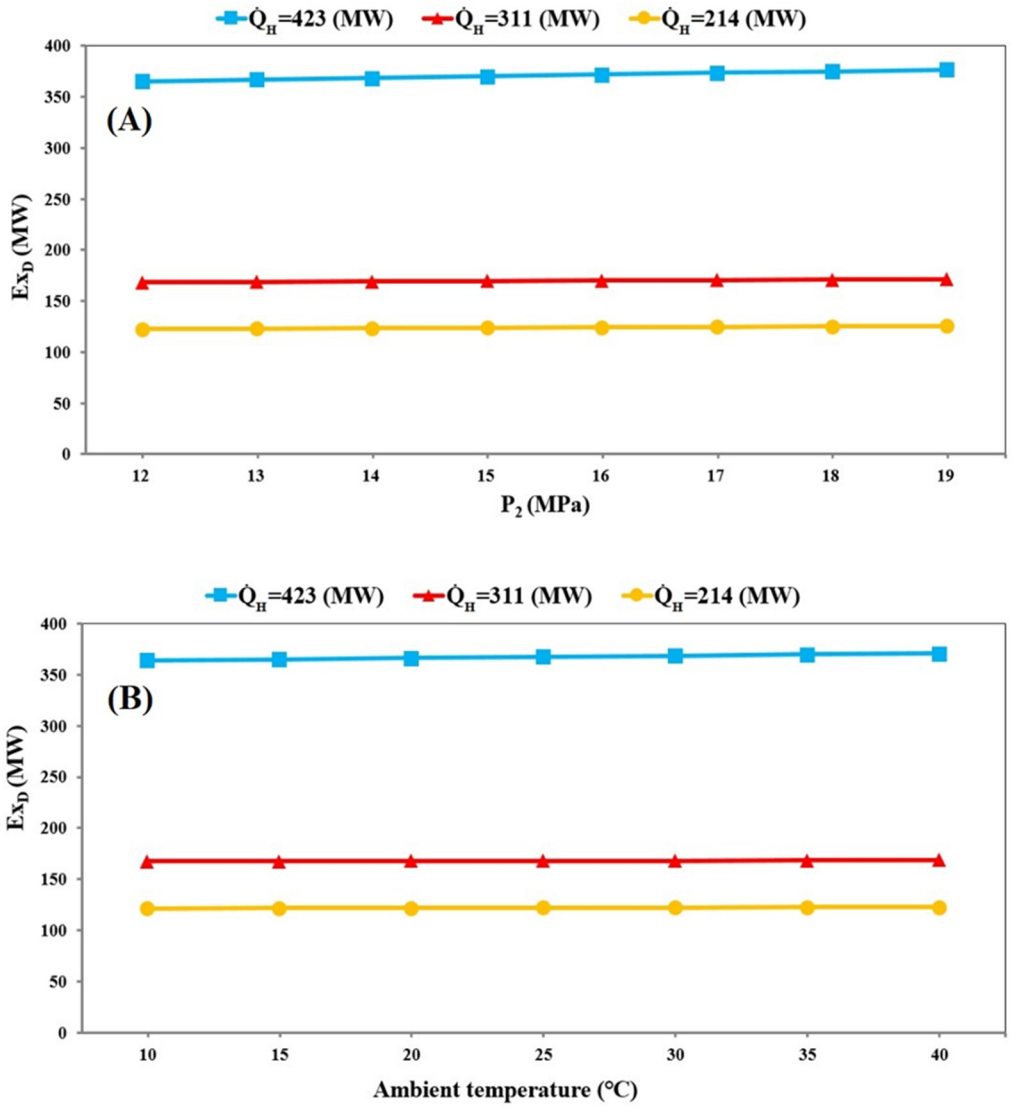

Figure 6. Variation in total exergy destruction with HP turbine inlet pressure (**A**) and ambient temperature (**B**).

3.3. Exergoeconomic Results

In this part, the total cost of the power plant and the exergetic efficiency against the inlet pressure of the turbine and the ambient temperature is illustrated in Figures 7 and 8. According to Figure 7, increasing the inlet pressure leads to lower exergy efficiency and lower total cost. At P_2 = 19 MPa and $\dot{Q}_H$ = 214 MW, the power plant has the lowest cost by 1.55 USD · h^{-1}. The highest heating load illustrates more sensitivity to the inlet pressure; increasing the pressure by 1 MPa results in a 1.64 USD·h^{-1} cost reduction. However, the highest heat load possesses medium exergetic efficiency: from 40.28% to 38.39% for the studied pressure range. At constant pressure, the intermediate heat load reveals higher exergy efficiency. At P_2 = 19 MPa, by decreasing the heat load by about 112 MW from the highest level, the exergy efficiency is enhanced by about 3.64%.

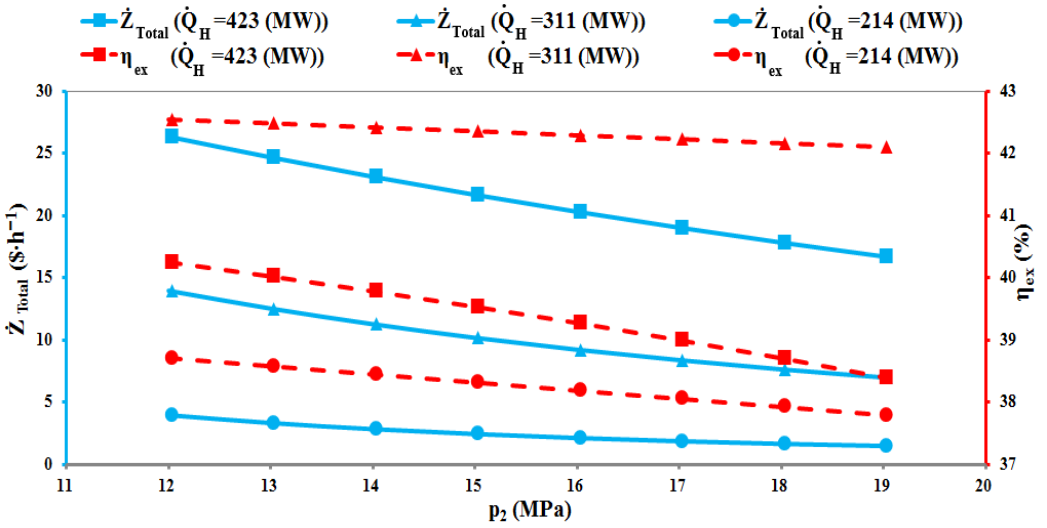

Figure 7. Variation in total cost and exergy efficiency with HP turbine inlet pressure.

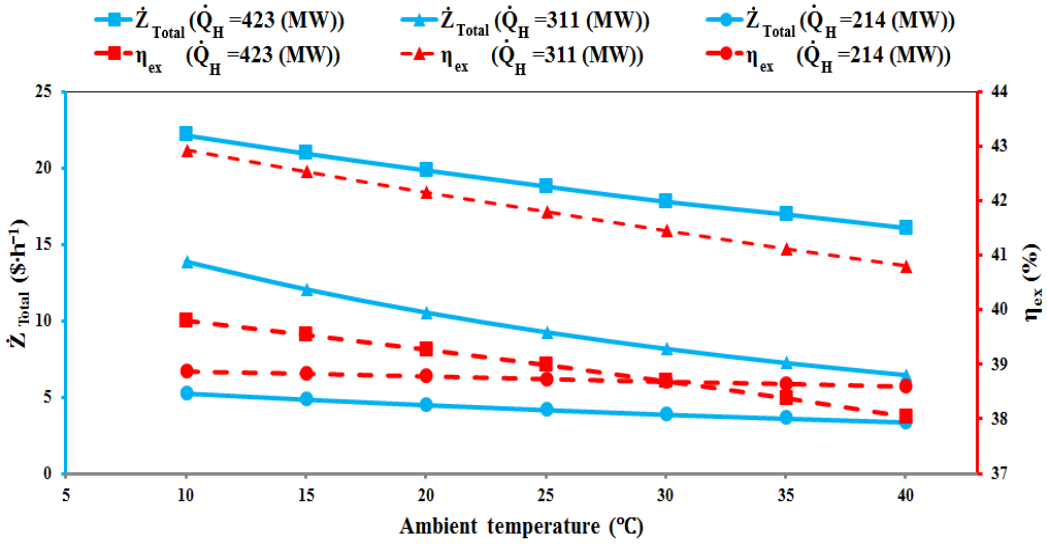

Figure 8. Variation in total cost and exergy efficiency with ambient temperature.

Increasing the ambient temperature for all the heat loads makes the power plant's total cost lower. A fourfold increase in the ambient temperature from the initial point T = 10 °C for $\dot{Q}_H$ = 311 MW drastically reduces the cost by about 6.17 USD·h^{-1}. The ambient temperature indirectly influences the exergetic performance. The heating load of 311 MW has the highest exergy efficiency for all the studied ambient temperatures. While the medium heat load from 10 °C to 30 °C shows higher exergy efficiency than $\dot{Q}_H$ = 214 MW, raising the ambient temperature to more than 30 °C leads to lower exergetic performance. The highest exergy efficiency is around 42.86% at 10 °C and $\dot{Q}_H$ = 311 MW.

The abovementioned results illustrate a trade-off between the three independent parameters and the studied performances, including work output, exergy efficiency, and the exergoeconomic indicator. Having an efficient power plant in terms of the highest performance at the lowest expenses calls for robust and precise optimization, which will be discussed in the next part.

3.4. Optimization Results

This section focuses on conducting a multi-criteria optimization considering ambient temperature and the inlet pressure of the HP turbine. Figure 9 depicts an optimal point demonstrating the highest exergy and work output coupled with the lowest overall system

cost achieved based on ambient temperature. For the highest heat load, $\dot{Q}_H$ = 423 MW, the optimal point for exergy efficiency, work output, and total cost is 38.9%, 151 MW, and 18.79 USD · h^{-1}, respectively. Ambient temperature has a greater impact on intermediate and low loads compared to high loads. Among the optimal points, the highest exergy efficiency of 42.15% occurs at the intermediate heat load ($\dot{Q}_H$ = 311 MW), the lowest total cost of USD 4.844 per hour occurs at the low heat load ($\dot{Q}_H$ = 214 MW), and the highest work output of 155.21 MW occurs at the high heat load ($\dot{Q}_H$ = 423 MW).

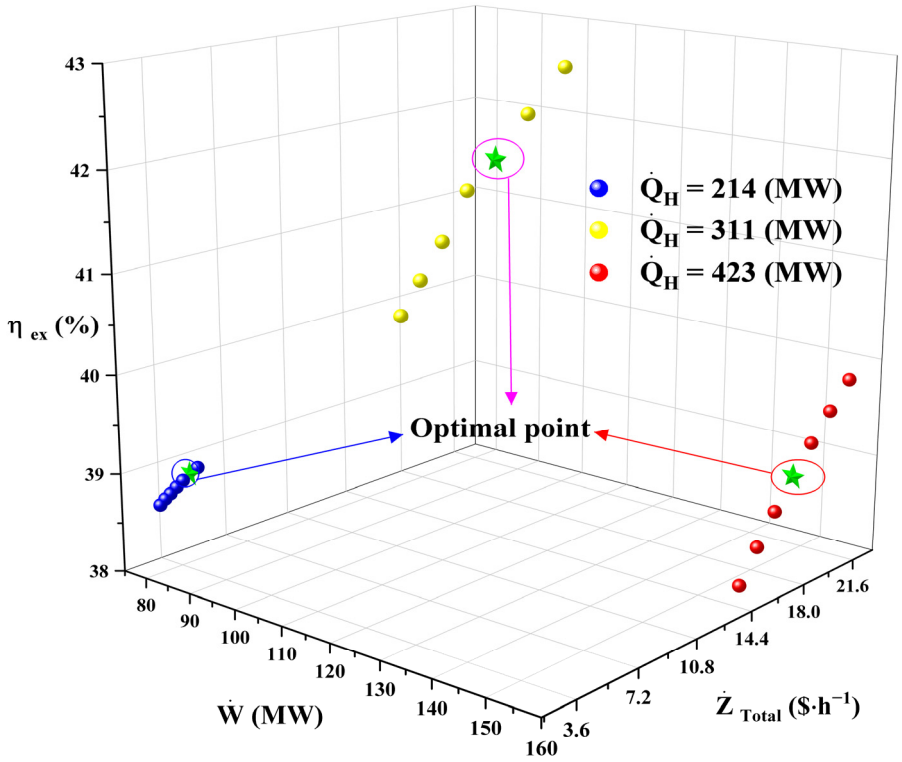

Figure 9. Multi-criteria optimization profile for different ambient temperatures.

Figure 10 displays the optimal points for all heat loads based on the turbine Hp inlet pressure within the range of 12 MPa to 19 MPa. Among the optimal points, the minimum total system cost for the heat load of $\dot{Q}_H$ = 214 MW is 1.668 USD · h^{-1}. As the heat load increases to the next level, $\dot{Q}_H$ = 311 MW, the power plant cost escalates fivefold, reaching 8.362 USD · h^{-1} under optimal conditions. Subsequently, this pattern is accompanied by a tenfold increase in cost, approximately 17.85 USD · h^{-1}, spanning from the lowest to the highest heat load. The highest exergy efficiency of 42.23% can be obtained at $\dot{Q}_H$ = 311 MW and 18 MPa. Decreasing the heat load by half, from $\dot{Q}_H$ = 423 MW to $\dot{Q}_H$ = 214 MW, leads to an almost 50% work output reduction from 150.77 MW to 74.17 MW at 18 MPa and 17 MPa in relation to the optimum situation.

Table 8 tabulates the exergoeconomic parameters for the various components used in the ejector refrigeration cycle. As observed, the highest cost is attributed to the condenser and the lowest is attributed to the expansion valve in the cycle.

The performance of the power plant, including work output, exergy efficiency, and total cost for the three distinct heat loads before and after optimization, is portrayed in Figure 11. Under optimal conditions, the work output increases by 16.37% at a heat load of $\dot{Q}_H$ = 214 MW. Notably, the exergy efficiency in the 423 MW heat load rises from 28% to 29.5%, and additionally, there is a 7.516 USD · h^{-1} difference in the total system cost between conventional and optimized conditions for this heat load.

Table 8. Exergoeconomic and cost parameters for different components of the proposed system.

Q = 214 MW							
Component	**C_f (USD·GJ^{-1})**	**Cp (USD·GJ^{-1})**	**$\dot{C}_D$ (USD·h^{-1})**	**$\dot{Z}_k$ (USD·h^{-1})**	**$\dot{C}_D + \dot{Z}_k$ (USD·h^{-1})**	**f (%)**	**r (%)**
Boiler	0.002621	0.6403	12.25	3.21	15.46	0.1429	2442
$Turbine_{HP}$	0.000256	0.001493	0.4032	0.06841	0.47161	0.1451	4.835
$Turbine_{IP}$	0.000006144	0.00002458	0.009083	0.06715	0.076233	0.8809	3
$Turbine_{LP}$	0.000006144	0.00001229	0.01016	0.01451	0.02467	0.5882	1
Condenser	0.000006144	0.00009125	0.2409	0.0004219	0.2413219	0.001748	13.85
$Pump_{cond}$	0.00008801	0.00009125	0.05181	0.0006064	0.0524164	0.01157	0.03691
LPH1	0.000005359	0.000006144	0.0004206	0.00001759	0.00043819	0.04014	0.1465
LPH2	0.000006144	0.000006364	0.00144	0.00005773	0.00149773	0.03854	0.0357
Deaerator	0.00000507	0.000005578	0.0008694	0.01131	0.0121794	0.9286	0.1001
BFP	0.000005201	0.000005516	0.02145	0.002486	0.023936	0.1039	0.06048
HPH1	0.000005099	0.000006144	0.001166	0.00004126	0.00120726	0.0001529	0.205
HPH2	0.001291	0.001238	0.3384	0.00005173	0.33845173	0.0401	0.0415
Q = 311 MW							
Component	**C_f (USD/GJ)**	**Cp (USD/GJ)**	**$\dot{C}_D$ (USD/h)**	**$\dot{Z}_k$ (USD/h)**	**$\dot{C}_D + \dot{Z}_k$ (USD/h)**	**f (%)**	**r (%)**
Boiler	0.0006933	0.9296	69	11.77	80.77	0.1457	1340
$Turbine_{HP}$	0.0006853	0.003275	1.506	0.06239	1.56839	0.03979	3.779
$Turbine_{IP}$	0.000007992	0.00003197	0.01764	0.1088	0.12644	0.8605	3
$Turbine_{LP}$	0.000007992	0.00001598	0.01552	0.04612	0.06164	0.7482	1
Condenser	0.000007992	0.0001131	0.4422	0.0005968	0.4427968	0.001348	13.15
$Pump_{cond}$	0.0001091	0.0001131	0.09041	0.0008004	0.0912104	0.008775	0.03602
LPH1	0.000006732	0.000007992	0.001414	0.00005694	0.00147094	0.03871	0.1871
LPH2	0.000007992	0.000007884	0.00166	0.00003532	0.00169532	0.02084	0.01353
Deaerator	0.000006212	0.000007075	0.005906	0.01467	0.020576	713	0.1388
BFP	0.000006382	0.000006418	0.03226	0.003232	0.035492	0.09105	0.005638
HPH1	0.000006485	0.000007992	0.001319	0.00002784	0.00134684	0.02067	0.2323
HPH2	0.002703	0.00259	1.095	0.00007558	1.09507558	0.00006903	0.04204
Q = 423 MW							
Component	**C_f (USD/GJ)**	**Cp (USD/GJ)**	**$\dot{C}_D$ (USD/h)**	**$\dot{Z}_k$ (USD/h)**	**$\dot{C}_D + \dot{Z}_k$ (USD/h)**	**f (%)**	**r (%)**
Boiler	0.0006377	1.285	85.45	17	102.45	0.166	2014
$Turbine_{HP}$	0.0006351	0.002489	1.987	0.04944	2.03644	0.02428	2.919
$Turbine_{IP}$	0.000002632	0.00001053	0.008034	0.1743	0.182334	0.9559	3
$Turbine_{LP}$	0.000002632	0.000005263	0.00651	0.03631	0.04282	0.848	1
Condenser	0.000002632	0.00003643	0.561	0.0008049	0.5618049	0.001441	12.85
$Pump_{cond}$	0.00003604	0.00003643	0.01281	0.0008923	0.0137023	0.06514	0.01103
LPH1	0.000002148	0.000002632	0.0008285	0.00009175	0.00092025	0.0997	0.2252
LPH2	0.000002632	0.000002763	0.002083	0.000174	0.002257	0.07711	0.04993
Deaerator	0.000002279	0.000002459	0.00523	0.01837	0.0236	0.7784	0.07891
BFP	0.000002344	0.000002508	0.01368	0.002984	0.016664	0.1791	0.07001
HPH1	0.000001669	0.000002632	0.0005317	0.00005685	0.00058855	0.0966	0.5763
HPH2	0.001233	0.001854	0.3256	0.00004935	0.32564935	0.0001515	0.504

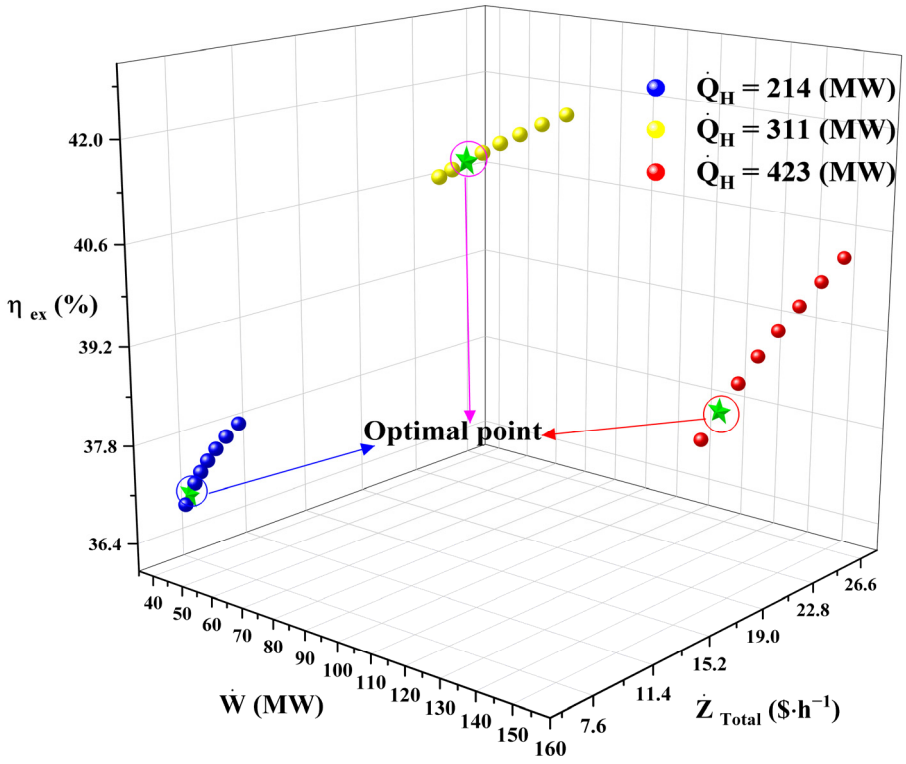

Figure 10. Multi-criteria optimization profile for different turbine inlet pressures.

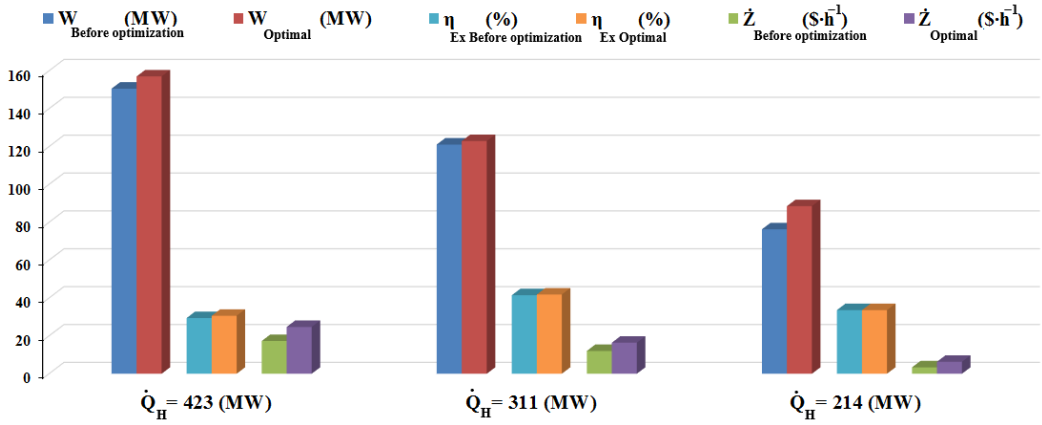

Figure 11. Work output, exergy efficiency, and cost analysis for different heat loads before and after optimization.

4. Conclusions

The thermodynamic performance of the Tous power plant, acknowledged as a significant energy source in northeastern Iran, has been thoroughly investigated and analyzed. This analysis focuses on energy, exergy, and exergoeconomic aspects. This study involved the multi-objective optimization of influential parameters through the employment of the TOPSIS method. To achieve this, the power plant was examined under three conditions: low load ($\dot{Q}_H$ = 214), intermediate load ($\dot{Q}_H$ = 311), and high load ($\dot{Q}_H$ = 423). In each of these scenarios, optimization was carried out for ambient temperature and inlet pressure into the high-pressure turbine. The most significant findings of this study are as follows:

- Ambient temperature has a greater impact on intermediate and low loads compared to high loads;
- In optimal conditions, the highest exergy efficiency of 42.15% occurs at the intermediate heat load;

- The power plant's output at a high thermal load stands at 145 MW, and after optimization this value escalates to 151 MW;
- The greatest improvement in power plant output is 16.37% for low thermal loads.
- The lowest cost reduction is related to the intermediate thermal load.

Author Contributions: Conceptualization, M.D.-D.; Methodology, M.T.; Validation, D.D.; Formal analysis, D.D.; Investigation, M.T.; Data curation, D.D.; Writing—original draft, M.T.; Writing—review & editing, B.M.-G.; Supervision, M.D.-D. All authors have read and agreed to the published version of the manuscript.

Funding: This research received no external funding.

Data Availability Statement: The data presented in this study are available on request from the corresponding author.

Acknowledgments: We would like to express our gratitude to the personnel of Mashhad Tous power plant in different sectors, including operation, repairs, and the technical office, for their sincere assistance in providing the flowsheets and technical information used in the current investigation.

Conflicts of Interest: The authors declare no conflict of interest.

Nomenclature

$\dot{c}$	cost per exergy (USD·kJ^{-1})
$\dot{Ex}_D$	exergy destruction (kW)
ex	specific exergy (kJ·kg^{-1})
i	interest
$\dot{m}$	mass flow rate (kg·s^{-1})
n	operating years
P	pressure (MPa)
$\dot{Q}$	heating power (kW)
s	specific entropy (kJ · kg^{-1}·K^{-1})
h	specific enthalpy (kJ · kg^{-1})
T	temperature (°C)
$\dot{W}$	shaft power (kW)
Z	purchase cost of the component (USD)
Subscripts	
b	boiler
c	condenser
en	energy
ex	exergy
in	inlet
out	outlet
RSH	re-super heat
SH	super heat
Greek letters	
ψ	calorific value of fuel (kW · kg^{-1})
η_{th}	energy efficiency
η_{ex}	exergy efficiency
γ	maintenance factor
τ	operating hour per year
Acronyms	
HPH	high-pressure heater
LPT	high-pressure turbine
IPT	intermediate-pressure turbine
LPH	low-pressure heater
BFP	boiler feed pump
CRF	capital recovery factor
CI	capital investment
OM	operating and maintenance

References

1. Kober, T.; Schiffer, H.-W.; Densing, M.; Panos, E. Global energy perspectives to 2060–WEC's World Energy Scenarios 2019. *Energy Strategy Rev.* **2020**, *31*, 100523.
2. Gholizadeh, M.; Deymi-Dashtebayaz, M.; Mehri, A.; Zameli, A.; Dadpour, D. Experimental evaluation and optimization of the anaerobic digestibility of two new desert weeds for biogas production. *Biomass Convers. Biorefinery* **2022**, 1–11. [CrossRef]
3. Ebrahimi-Moghadam, A.; Deymi-Dashtebayaz, M.; Jafari, H.; Niazmand, A. Energetic, exergetic, environmental and economic assessment of a novel control system for indirect heaters in natural gas city gate stations. *J. Therm. Anal. Calorim.* **2020**, *141*, 2573–2588.
4. Tayyeban, E.; Deymi-Dashtebayaz, M.; Dadpour, D. Multi objective optimization of MSF and MSF-TVC desalination systems with using the surplus low-pressure steam (an energy, exergy and economic analysis). *Comput. Chem. Eng.* **2022**, *160*, 107708.
5. Farhadi, F.; Deymi-Dashtebayaz, M.; Tayyeban, E. Studying a Multi-Stage Flash Brine Recirculation (MSF-BR) System Based on Energy, Exergy and Exergoeconomic Analysis. *Water* **2022**, *14*, 3108.
6. Kabiri, M.; Akbarpour, A.; Akbari, M. Evaluation of the efficiency of a gray water treatment system based on aeration and filtration. *J. Water Reuse Desalination* **2021**, *11*, 361–372.
7. Kaushik, S.; Reddy, V.S.; Tyagi, S. Energy and exergy analyses of thermal power plants: A review. *Renew. Sustain. Energy Rev.* **2011**, *15*, 1857–1872.
8. Chen, T.-C.; Kumar, T.C.A.; Dwijendra, N.K.A.; Majdi, A.; Asary, A.R.; Iswanto, A.H.; Khan, I.; Madsen, D.Ø.; Alayi, R. Energy and Exergy Analysis of the Impact of Renewable Energy with Combined Solid Oxide Fuel Cell and Micro-Gas Turbine on Poly-Generation Smart-Grids. *Water* **2023**, *15*, 1069.
9. Amiralipour, M.; Kouhikamali, R. Guilan combined power plant in Iran: As case study for feasibility investigation of converting the combined power plant into water and power unit. *Energy* **2020**, *201*, 117656.
10. Lin, X.; Li, Q.; Wang, L.; Guo, Y.; Liu, Y. Thermo-economic analysis of typical thermal systems and corresponding novel system for a 1000 MW single reheat ultra-supercritical thermal power plant. *Energy* **2020**, *201*, 117560.
11. Owebor, K.; Diemuodeke, E.; Briggs, T. Thermo-economic and environmental analysis of integrated power plant with carbon capture and storage technology. *Energy* **2022**, *240*, 122748.
12. Zahedi, R.; Ahmadi, A.; Dashti, R. Energy, exergy, exergoeconomic and exergoenvironmental analysis and optimization of quadruple combined solar, biogas, SRC and ORC cycles with methane system. *Renew. Sustain. Energy Rev.* **2021**, *150*, 111420.
13. Abbaspour, H.; Ehyaei, M.; Ahmadi, A.; Panahi, M.; Abdalisousan, A.; Mirzohosseini, A. Energy, exergy, economic, exergoenvironmental and environmental (5E) analyses of the cogeneration plant to produce electrical power and urea. *Energy Convers. Manag.* **2021**, *235*, 113951.
14. Topal, H.; Taner, T.; Naqvi, S.A.H.; Altınsoy, Y.; Amirabedin, E.; Ozkaymak, M. Exergy analysis of a circulating fluidized bed power plant co-firing with olive pits: A case study of power plant in Turkey. *Energy* **2017**, *140*, 40–46.
15. Mohammadpour, M.; Houshfar, E.; Ashjaee, M.; Mohammadpour, A. Energy and exergy analysis of biogas fired regenerative gas turbine cycle with CO_2 recirculation for oxy-fuel combustion power generation. *Energy* **2021**, *220*, 119687.
16. Abuelnuor, A.; Saqr, K.M.; Mohieldein, S.A.A.; Dafallah, K.A.; Abdullah, M.M.; Nogoud, Y.A.M. Exergy analysis of Garri "2" 180 MW combined cycle power plant. *Renew. Sustain. Energy Rev.* **2017**, *79*, 960–969.
17. Bai, W.; Li, H.; Zhang, L.; Zhang, Y.; Yang, Y.; Zhang, C.; Yao, M. Energy and exergy analyses of an improved recompression supercritical CO_2 cycle for coal-fired power plant. *Energy* **2021**, *222*, 119976.
18. Yan, H.; Liu, M.; Chong, D.; Wang, C.; Yan, J. Dynamic performance and control strategy comparison of a solar-aided coal-fired power plant based on energy and exergy analyses. *Energy* **2021**, *236*, 121515.
19. Shamoushaki, M.; Fiaschi, D.; Manfrida, G.; Talluri, L. Energy, exergy, economic and environmental (4E) analyses of a geothermal power plant with NCGs reinjection. *Energy* **2021**, 122678.
20. Elhelw, M.; Al Dahma, K.S. Utilizing exergy analysis in studying the performance of steam power plant at two different operation mode. *Appl. Therm. Eng.* **2019**, *150*, 285–293.
21. Khaleel, O.J.; Ibrahim, T.K.; Ismail, F.B.; Al-Sammarraie, A.T. Developing an analytical model to predict the energy and exergy based performances of a coal-fired thermal power plant. *Case Stud. Therm. Eng.* **2021**, *28*, 101519.
22. Ahmadi, G.; Toghraie, D.; Akbari, O. Energy, exergy and environmental (3E) analysis of the existing CHP system in a petrochemical plant. *Renew. Sustain. Energy Rev.* **2019**, *99*, 234–242.
23. Adnan, A.; Mahmud, S.; Uddin, M.R.; Modi, A.; Ehsan, M.M.; Salehin, S. Energy, Exergy, Exergoeconomic, and environmental (4E) analyses of thermal power plants for municipal solid waste to energy application in Bangladesh. *Waste Manag.* **2021**, *134*, 136–148.
24. Hao, R.; Qiao, L.; Han, L.; Tian, C. Experimental study on the effect of heat-retaining and diversion facilities on thermal discharge from a power plant. *Water* **2020**, *12*, 2267.
25. Dadpour, D.; Gholizadeh, M.; Estiri, M.; Poncet, S. Multi objective optimization and 3E analyses of a novel supercritical/transcritical CO_2 waste heat recovery from a ship exhaust. *Energy* **2023**, *278*, 127843.
26. Dadpour, D.; Gholizadeh, M.; Lakzian, E.; Delpisheh, M.; Kim, H.D. Vehicle refrigeration modification using an ejector: Optimization and exergoeconomic analysis. *J. Taiwan Inst. Chem. Eng.* **2023**, *148*, 104875. [CrossRef]
27. Akhoundi, M.; Deymi-Dashtebayaz, M.; Tayyeban, E.; Khabbazi, H. Parametric study and optimization of the precooled Linde–Hampson (PCLH) cycle for six different gases based on energy and exergy analysis. *Chem. Pap.* **2023**, 1–14. [CrossRef]

28. Hekmatshoar, M.; Deymi-Dashtebayaz, M.; Gholizadeh, M.; Dadpour, D.; Delpisheh, M. Thermoeconomic analysis and optimization of a geothermal-driven multi-generation system producing power, freshwater, and hydrogen. *Energy* **2022**, *247*, 123434.
29. Deymi-Dashtebayaz, M.; Sulin, A.; Ryabova, T.; Sankina, I.; Farahnak, M.; Nazeri, R. Energy, exergoeconomic and environmental optimization of a cascade refrigeration system using different low GWP refrigerants. *J. Environ. Chem. Eng.* **2021**, *9*, 106473.
30. Lazzaretto, A.; Tsatsaronis, G. SPECO: A systematic and general methodology for calculating efficiencies and costs in thermal systems. *Energy* **2006**, *31*, 1257–1289.
31. Sami, S.; Gholizadeh, M.; Dadpour, D.; Deymi-Dashtebayaz, M. Design and optimization of a CCHDP system integrated with NZEB from energy, exergy and exergoeconomic perspectives. *Energy Convers. Manag.* **2022**, *271*, 116347.
32. Ghorbani, S.; Deymi-Dashtebayaz, M.; Tayyeban, E. Parametric investigation and performance optimization of a MED-TVC desalination system based on 1-D ejector modeling. *Energy Convers. Manag.* **2023**, *288*, 117131.
33. Habibollahzade, A.; Petersen, K.; Aliahmadi, M.; Fakhari, I.; Brinkerhoff, J. Comparative thermoeconomic analysis of geothermal energy recovery via super/transcritical CO2 and subcritical organic Rankine cycles. *Energy Convers. Manag.* **2022**, *251*, 115008.
34. Hajabdollahi, F.; Hajabdollahi, Z.; Hajabdollahi, H. Soft computing based multi-objective optimization of steam cycle power plant using NSGA-II and ANN. *Appl. Soft Comput.* **2012**, *12*, 3648–3655.
35. Ghorbani, S.; Deymi-Dashtebayaz, M.; Dadpour, D.; Delpisheh, M. Parametric study and optimization of a novel geothermal-driven combined cooling, heating, and power (CCHP) system. *Energy* **2023**, *263*, 126143.
36. Deymi-Dashtebayaz, M.; Dadpour, D.; Khadem, J. Using the potential of energy losses in gas pressure reduction stations for producing power and fresh water. *Desalination* **2021**, *497*, 114763.
37. Dadpour, D.; Deymi-Dashtebayaz, M.; Hoseini-Modaghegh, A.; Abbaszadeh-Bajgiran, M.; Soltaniyan, S.; Tayyeban, E. Proposing a new method for waste heat recovery from the internal combustion engine for the double-effect direct-fired absorption chiller. *Appl. Therm. Eng.* **2022**, *216*, 119114.
38. Nikitin, A.; Farahnak, M.; Deymi-Dashtebayaz, M.; Muraveinikov, S.; Nikitina, V.; Nazeri, R. Effect of ice thickness and snow cover depth on performance optimization of ground source heat pump based on the energy, exergy, economic and environmental analysis. *Renew. Energy* **2022**, *185*, 1301–1317.